The Journal of Neuroscience, May 1, 2001, 21(9):3034–3044

Drosophila Stoned Proteins Regulate the Rate and Fidelity of Synaptic Vesicle Internalization

Daniel T. Stimson,[1] Patricia S. Estes,[1] Sujata Rao,[3] K. S. Krishnan,[3] Leonard E. Kelly,[2] and Mani Ramaswami[1]

[1]Department of Molecular and Cellular Biology and Arizona Research Laboratories Division of Neurobiology, University of Arizona, Tucson, Arizona 85721, [2]Department of Genetics, University of Melbourne, Parkville, Australia, and [3]Department of Biological Sciences, Tata Institute of Fundamental Research, Bombay, India

At an initial step during synaptic vesicle recycling, dynamin and adaptor proteins mediate the endocytosis of synaptic vesicle components from the plasma membrane. StonedA and stonedB, novel synaptic proteins encoded by a single *Drosophila* gene, have predicted structural similarities to adaptors and other proteins implicated in endocytosis. Here, we test possible roles of the stoned proteins in synaptic vesicle internalization via analyses of third instar larval neuromuscular synapses in two *Drosophila stoned* (*stn*) mutants, stn^{ts} and stn^{8P1}. Both mutations reduce presynaptic levels of stonedA and stonedB, although stn^{ts} has relatively weak effects. The mutations cause retention of synaptic vesicle proteins on the presynaptic plasma membrane but do not alter the levels or distribution of endocytosis proteins, dynamin, α-adaptin, and clathrin. In addition, stn^{8P1} mutants exhibit depletion and enlargement of synaptic vesicles. To determine whether these defects arise from altered synaptic vesicle endocytosis or from defects in synaptic vesicle biogenesis, we implemented new methods to assess directly the efficiency of synaptic vesicle recycling and membrane internalization at *Drosophila* nerve terminals. Behavioral and electrophysiological analyses indicate that stn^{ts}, an allele with normal evoked release and synaptic vesicle number, enhances defects in synaptic vesicle recycling shown by *Drosophila* shi^{ts} mutants. A dye uptake assay demonstrates that slow synaptic vesicle recycling in stn^{ts} is accompanied by a reduced rate of synaptic vesicle internalization after exocytosis. These observations are consistent with a model in which stonedA and stonedB act to facilitate the internalization of synaptic vesicle components from the plasma membrane.

Key words: stonedA; stonedB; adaptins; shibire*; dynamin; larval neuromuscular junction*

After exocytosis the coordinated endocytosis of synaptic vesicle membrane proteins is mediated by adaptor proteins, including AP180 (Zhang et al., 1998; Nonet et al., 1999) and the AP-2 complex, a tetramer consisting of α, β, μ, and σ subunit proteins (Robinson, 1992; Zhang et al., 1994; Gonzalez-Gaitan and Jackle, 1997). These adaptor proteins bind the cytoplasmic tails of synaptic vesicle membrane proteins displayed on the plasma membrane (Zhang et al., 1994; De Camilli and Takei, 1996). Simultaneously, they facilitate assembly of the coat protein clathrin into homogeneously sized cages (Shih et al., 1995; Ye and Lafer, 1995), a process that probably helps to drive membrane invagination (Robinson, 1994). Subsequently, vesicle fission and internalization from the plasma membrane occur via constriction of the "neck" of the budding vesicle by the GTPase dynamin and other associated proteins (Takei et al., 1995; Warnock and Schmid, 1996; Schmid et al., 1998). Several additional proteins probably participate in regulating the various stages of endocytic vesicle formation.

The *Drosophila stoned* locus encodes two novel proteins for which the sequences suggest that they might be specialized adaptors (Andrews et al., 1996). A dicistronic *stoned* mRNA contains two open reading frames (ORFs): the 5′ ORF (ORF1) encodes stonedA, and the 3′ ORF (ORF2) produces a structurally unrelated protein, stonedB (Andrews et al., 1996). Both proteins are enriched at *Drosophila* nerve terminals (Stimson et al., 1998; Fergestad et al., 1999). Although stonedA has no extended homology to known proteins, stonedB contains a C-terminal domain that is ~40% identical to the μ-adaptin family (Robinson, 1992; Andrews et al., 1996). In addition, stonedA and stonedB contain distinct tripeptide repeats (DPF and NPF) known to serve as functionally important motifs in the adaptor-associated proteins Eps15 and synaptojanin, respectively (Salcini et al., 1997; Stimson et al., 1998).

Previous phenotypic studies of *Drosophila stoned* mutants have provided evidence to suggest that stoned proteins regulate synaptic vesicle recycling. First, stn^{ts} and shi^{ts1}, a mutation disrupting *Drosophila* dynamin, show synthetic lethality, a genetic interaction suggestive of common biological function for *stn* and *shi* (Chen et al., 1991; van der Bliek and Meyerowtiz, 1991; Petrovich et al., 1993). Second, several *stoned* mutations disrupt neurotrans-

Received Aug. 22, 2000; revised Jan. 16, 2001; accepted Jan. 24, 2001.

This work was funded by National Institutes of Health Grants NS34889 and KO2-NS02001 to M.R., by the McKnight Foundation and Alfred P. Sloan Foundation, by a Human Frontier Science Program grant to M.R. and L.E.K. (and four others), and by Grant 960117 from the National Health and Medical Research Council (Australia) to L.E.K. D.T.S. acknowledges support from Developmental Neuroscience Research Training grants at the University of Arizona, funded by the Flinn Foundation and the National Institutes of Health. We thank A. Marie Phillips, Dave Sandstrom, and members of the Ramaswami lab for useful discussions and T. McCormack for the identification of PEST sequences in stonedB. We are grateful to Rick Levine and the Levine lab for help with electrophysiology. We thank Patty Jansma for assistance with confocal and electron microscopy (EM), performed with microscopes belonging to the Arizona Research Laboratories (ARL) Division of Neurobiology. We also thank Gina Zhang of the ARL Division of Biotechnology Imaging Facility for help with EM thin sections and Charles (Chip) Hedgcock, Registered Biological Photographer, for help with EM micrographs. We are grateful to Troy Littleton and Hugo Bellen for anti-Syt antibodies, Erich Buchner and Konrad Zinsmaier for anti-Csp antibodies, Jack Roos and Reg Kelly for anti-dynamin, and Saffron Dornan and Nick Gay for anti-α-adaptin antibodies.

Correspondence should be addressed to Dr. Mani Ramaswami, Department of Molecular and Cellular Biology, Life Sciences South Room 444, University of Arizona, P.O. Box 210106, Tucson, AZ 85721. E-mail: mani@u.arizona.edu.

mitter release and cause redistribution of the synaptic vesicle membrane protein synaptotagmin (Syt) to the presynaptic plasma membrane (Stimson et al., 1998; Fergestad et al., 1999). Finally, lethal *stoned* mutations alter the density and size of synaptic vesicles at the embryonic neuromuscular junction (NMJ; Fergestad et al., 1999). Although these observations suggest that stoned proteins facilitate synaptic vesicle recycling, they fall short of demonstrating altered vesicle recycling in *stoned* mutants. The stage of synaptic vesicle traffic at which stoned proteins function remains unknown. Also yet to be resolved is whether *stoned* is required for selective traffic of synaptotagmin (Fergestad et al., 1999) or also for traffic of other vesicle proteins. Here, we address these issues by new analyses of a viable allele, stn^{ts}, and a "semi-lethal" allele, stn^{8P1}.

As in other *stoned* lethal mutants, synaptic vesicles are depleted and enlarged in stn^{8P1} terminals. Immunofluorescence analyses, possible at large presynaptic endings (boutons) of the larval NMJ, show that *stn* mutations cause enhanced retention of two synaptic vesicle proteins, Syt and cysteine string protein (Csp), on the presynaptic plasma membrane without altering the distribution or levels of the endocytosis proteins, dynamin, clathrin and α-adaptin. New physiological assays show that the stn^{ts} mutation, which affects neither evoked release nor synaptic vesicle number at the larval synapse, slows the rate of dynamin-dependent recycling as well as the rate of synaptic vesicle internalization. On the basis of these findings, we propose that stoned proteins are novel components of endocytic vesicle formation that facilitate the internalization of multiple synaptic vesicle proteins from plasma membrane.

MATERIALS AND METHODS

Drosophila *strains and genetics*

Drosophila cultures were raised at 21°C under noncrowded conditions as described previously (Stimson et al., 1998). The *Oregon-R* strain was used as a wild-type control. The hypomorphic stn^{ts} and lethal $stn^{13–120}$ alleles were from our collection. The stn^{ts} mutation, originally called stn^{ts2}, was generated in the same genetic screen that yielded another *stoned* allele, stn^{ts1} (Grigliatti et al., 1973). Sequencing of genomic DNA from both mutants indicates that they are genetically identical at the *stoned* locus (Phillips et al., 2000); therefore, this single *stoned* allele is referred to as stn^{ts}. The semi-lethal stn^{8P1} mutation was provided by Norbert Perrimon (Howard Hughes Medical Institute, Harvard Medical School, Boston, MA). We generated *shi–stn* double mutant chromosomes, including shi^{ts2} *f* stn^{ts}, shi^{ts4} *f* stn^{ts}, and shi^{ts2} $stn^{13–120}$, using marker replacement to screen recombinants.

The stn^{ts} mutant was maintained as a homozygous stock. The shi^{ts2} *f* stn^{ts} and shi^{ts4} *f* stn^{ts} double mutants were maintained as heterozygous stocks by using either the *FM7* balancer, which carries the *Bar* mutation, or *FM7i* (Bloomington Stock Center, number 4559), which additionally contains a transgene for the jellyfish green fluorescent protein (GFP), driven by a cytoplasmic *actin* promoter. The stn^{8P1} and shi^{ts2} *f* $stn^{13–120}$ mutants were maintained over the modified Y chromosome $Dp(1,Y)y^{+}$ $Ymal^{+}$ (abbreviated in text and figures as *Dp*), which contains a duplication of a segment of the proximal X chromosome that includes the entire *stoned* locus. The $stn^{13–120}$ mutant was maintained over both *FM7i* and $Dp(1,Y)y^{+}Ymal^{+}$ in two stocks.

To generate stn^{8P1} mutant larvae, we crossed stn^{8P1}/Dp males to *yfC(1)DX/Y* (attached-X) females, yielding males of the genotype stn^{8P1}/Y. Shi^{ts2} *f* stn^{ts} mutant flies were selected from the shi^{ts2} *f* stn^{ts}/*FM7i* stock based on the absence of the *Bar* phenotype. Shi^{ts2} *f* stn^{ts} mutant larvae were obtained by selecting nongreen fluorescent larvae from the shi^{ts2} *f* stn^{ts}/*FM7i* stock, using a Leica stereo microscope with a GFP fluorescence illuminator (Kramer Scientific, Elmsford, NY). Absence of green fluorescence also was used to select $stn^{8P1}/stn^{13–120}$ and shi^{ts2} *f* stn^{ts}/shi^{ts2} $stn^{13–120}$ larval progeny from the appropriate crosses.

Adult paralysis

Paralysis was assayed as previously described (Ramaswami et al., 1993; Grant et al., 1998). Approximately 6–30 flies were loaded into a water-jacketed glass chamber held at different temperatures. The number of paralyzed flies was noted at varying time points 0–5 min after introduction into the chamber. Between experiments the flies were allowed to recover for at least 10 min at 18–20°C. The flies that were tested were between 2 and 4 d of age. The restrictive temperature is defined as the temperature at which 100% of the flies are paralyzed in 2 min.

Larval neuromuscular preparations

For electrophysiology and microscopy of larval neuromuscular synapses, larvae were dissected to expose the bilaterally and segmentally iterated body wall muscles (Stimson et al., 1998). Larval dissections were performed in Ca^{2+}-free saline (see Physiology below) containing 0.5 mM EGTA and 21.5 mM $MgCl_2$ (HL3 saline) to prevent muscle contraction. Analyses were restricted to synapses of muscles 6 and 7 of abdominal segments 2–4 (A2–A4). These synapses are formed by a pair of identified motor neurons and have been used extensively in studies of synapse function and structure in *Drosophila* (Keshishian et al., 1996; Littleton et al., 1999).

Electrophysiology

Recordings of excitatory junctional potentials (EJPs) and miniature excitatory junctional potentials (mejps) were performed as described previously (Stimson et al., 1998) at room temperature (22°C), unless otherwise specified. The CNS was cut away from the dissected preparation, and the Ca^{2+}-free saline was replaced with normal HL3 saline, pH 7.2, containing (in mM) 70 NaCl, 5 KCl, 21.5 $MgCl_2$, 10 $NaHCO_3$, 5 trehalose, 115 sucrose, and 5 HEPES, pH 7.3 (Stewart et al., 1994). Intracellular recordings were made by impaling muscle 6 of A3 with sharp microelectrodes. Microelectrodes were pulled from borosilicate capillary tubes (1.0 mm outer diameter and 0.5 mm inner diameter; Friedrich & Dimmock, Millville, NJ) and filled with 2 M KAc, with resulting tip resistances of 20–45 MΩ. To elicit EJPs, we drew the free end of the nerve innervating an A3 hemi-segment into a suction electrode with a 10 μm diameter tip and stimulated it with an isolated pulse stimulator (A-M Systems, Everett, WA).

Synaptic physiology of stn^{8P1}. Compound EJPs, which reflect the activity of both motor neurons that innervate muscle 6, were elicited by 1 msec stimuli delivered at a frequency of 1 Hz and an intensity ~1.5× the required threshold. The EJP amplitude of a given larval preparation was determined by averaging 25 EJPs. Recordings were taken by using an Axoclamp 2B amplifier in conjunction with pClamp 6.0 software (Axon Instruments, Foster City, CA). To quantify the frequency of spontaneous vesicle fusion events, we counted mejps within a 30 sec block of recording from each larva. For determining mean mejp amplitudes in stn^{8P1} and stn^{8P1}/Dp, we took measurements only from recordings with a stable membrane potential (V_m) between −60 and −76 mV. For these preparations the average V_m values in stn^{8P1} and stn^{8P1}/Dp were −67 ± 2.0 and −70 ± 1.9 mV, respectively, and were not significantly different. Frequency distributions over an equivalent range of mejp amplitudes for stn^{8P1}/Y and $stn^{8P1}/mal^{+}Y$ were created by using dummy values of 0.1 and 7.5 mV for the bins at the extreme ends of each distribution. To determine whether maximal mejp size in the stn^{8P1} mutant is limited by a decrease in postsynaptic sensitivity, we tested the response of stn^{8P1} muscle to iontophoretically applied glutamate. Although we always observed robust responses in stn^{8P1} and stn^{8P1}/Dp, the responses were often much larger than normal EJPs. Thus, the technique probably was not sensitive enough to detect small decreases in glutamate receptor density.

Depression experiments. Using magnetically attached pins, we dissected and positioned larvae on a glass slide tightly clamped on a custom-designed stage, which could be heated and cooled with a Peltier temperature controller (Physitemp, Clifton, NJ). Using a thermocouple microprobe (Physitemp) to monitor bath temperature, we heated the bath to 28 or 30°C, and then impaled muscle 6 for intracellular recording. EJPs were elicited by stimuli delivered at 10 Hz and were recorded with Axoscope 1.0 software (Axon Instruments). The combination of high temperature and high frequency stimulation occasionally led to nerve conduction failure in the larval preparation. Oxygenation via a fish tank aerator did not abolish this sporadic conduction failure. Therefore, to ensure continuous nerve activity, we increased the stimulus pulse duration to 5 msec and carefully monitored EJPs to verify recruitment of both motor neurons, adjusting the stimulus intensity as necessary. To assess

depression in each larval preparation, we determined EJP amplitudes by taking the average of five measurements for each time interval over a time course divided into 30 sec intervals. Using a correction factor to account for nonlinear summation of quanta (Martin, 1955), we calculated quantal content for each time point in a single preparation by dividing the EJP amplitude by the average mejp amplitude.

Electron microscopy

Larval preparations were processed as described previously (Stimson et al., 1998) and examined under a Jeol 1200EX electron microscope (Peabody, MA). Only type I boutons (Johansen et al., 1989; Atwood et al., 1993) of muscle 6 or 7 in A2–A4 were used for analysis. Density and size of synaptic vesicles were determined by manual measurements from profiles containing subsynaptic reticulum and at least one active zone.

Antibodies, immunohistochemistry, and confocal microscopy

Dissected larvae were fixed in 3.5% paraformaldehyde and processed for antibody staining by previously described procedures (Estes et al., 1996; Stimson et al., 1998), except for anti-clathrin staining for which we used Bouin's fixative (15:5:1 saturated picric acid, 37% paraformaldehyde, glacial acetic acid) for 20 min. A PCM-2000 laser-scanning confocal microscope (Nikon, Melville, NY) and Simple32 software (C Imaging, Cranberry Township, PA) or a Bio-Rad 600 confocal microscope and COMOS software (Bio-Rad, Richmond, CA) were used for image acquisition.

StonedA antiserum, described previously (Stimson et al., 1998), was used at a final dilution of 1:1000. StonedB antiserum was generated in collaboration with Alpha Diagnostic International (San Antonio, TX) as follows. Antigenic stonedB peptides were designed by identifying amino acid sequences of optimal antigenicity, hydrophilicity, and accessibility for antibody binding. After protein regions conserved between stonedB and homologous proteins were eliminated from consideration, two optimal peptides were selected and synthesized: stnb 89 (amino acids 89–104) and stnb 1244 (amino acids 1244–1262). To stimulate the production of large antibody titers, we conjugated both peptides to KLH and simultaneously injected them into two rabbits (numbers 3500 and 3501). For both antisera 3500 and 3501, ELISA assays revealed the presence of antibodies to each peptide, and immunohistochemistry yielded staining of synaptic boutons at the larval NMJ. Peptide preadsorption experiments showed that the stnb 89 peptide eliminated antiserum 3500 immunostaining, but neither peptide eliminated antiserum 3501 immunostaining. Therefore, for all immunohistochemistry experiments we used antiserum 3500 at a final dilution of 1:500. Anti-stonedB and anti-stonedA were visualized by using a Texas Red-conjugated goat anti-rabbit antibody (ICN Biochemicals, Costa Mesa, CA) at a 1:200 dilution.

For comparing the distributions of synaptotagmin and Csp within synaptic boutons, we double-stained the larval preparation with rabbit anti-Syt antibody (DSYT2; from Hugo Bellen, Baylor College of Medicine, Houston, TX) and mouse anti-Csp antibody (Ab 49; from Konrad Zinsmaier, University of Pennsylvania School of Medicine, Philadelphia, PA). Goat anti-clathrin antibodies were from Sigma (St. Louis, MO), rabbit anti-dynamin (2074) was from Jack Roos (University of California, San Francisco, CA) and rat anti-α-adaptin (SD101) was from Saffron Dornan and Nick Gay (University of Cambridge, Cambridge, UK). Antibody dilutions (1:200 for DSYT2, 1:20–1:50 for Ab 49, 1:100 for clathrin, 1:200 for 2074, and 1:200 for SD101) were optimized to match staining intensities. Anti-Syt and anti-Csp were visualized simultaneously by using appropriate secondary antibodies conjugated to red (Texas Red, ICN Biochemicals) and green (FITC, ICN Biochemicals; Alexa 488, Molecular Probes, Eugene, OR) fluorophores. Confocal sections, 0.5–1 μm thick, were collected at 60× power, 5× zoom, using the K1/K2 filter supplied by Bio-Rad to view the red and green channels simultaneously. We carefully controlled for bleed-through by matching staining intensities and by doing single-stained controls to calibrate the confocal microscope.

FM1-43 uptake experiments

To promote synaptic vesicle endocytosis and uptake of FM1-43 (Molecular Probes) within boutons innervating muscles 6 and 7, we stimulated a single A3 hemi-segment at 10 V, 30 Hz for 30 sec (buzz). To monitor endocytosis, we applied 4 μM FM1-43 just before the stimulation at $t = 0$ or at $t = 1$ min after stimulation. After 5 min of FM1-43 incubation without stimulation, noninternalized FM1-43 was washed away by using Ca^{2+}-free HL3 saline in two quick washes and then four 5 min washes. Immediately after washing, the stained boutons were viewed under a fluorescence compound microscope (Zeiss, Frankfurt, Germany), and digital images were acquired with a cooled CCD camera (Princeton Instruments, Trenton, NJ) controlled by MetaMorph imaging software (Universal Imaging, West Chester, PA). Occasionally, stained boutons appeared in nonstimulated hemi-segments, and these preparations were discarded. To obtain images of the highest possible resolution, we performed quantitative fluorescent measurements only on type Ib boutons [large boutons ranging 2–5 μm in diameter (Johansen et al., 1989; Atwood et al., 1993)] on the surfaces of muscles 6 and 7. Background fluorescence from muscle surface close to the boutons was subtracted from each image, and then fluorescence intensity (average pixel value) was measured for each Ib bouton that was clearly in focus. Each larva was used only once for a single time point.

The fraction of synaptic vesicle internalized during the buzz, versus at time points 0 or 1 min after the buzz, was determined by dividing the pixel value obtained for each time point by the maximal dye uptake for that genotype. Maximal uptake (dye present during the 30 Hz stimulation) as well as during recovery was 1135 ± 76 (for control) compared with 746 ± 82 in stn^{ts} and 369 ± 38 in stn^{ts}/stn^{13-120}. Pixel values for boutons when FM1-43 was applied at $t = 0$ (just after stimulation) were 427 ± 16 (for control) compared with 467 ± 44 for stn^{ts} and 261 ± 37 for stn^{ts}/stn^{13-120}; for $t = 1$ min the pixel values were 63 ± 34, 181 ± 33, and 198 ± 10 for the three genotypes, respectively. Reduced maximal dye uptake in *stoned* mutants likely derives from lower total synaptic vesicle exocytosis during the 30 Hz buzz; this is consistent with the depression traces shown in Figure 6*D*.

Data analysis and statistics

In the text and in figures the error measurements are shown as SEM. Statistical significance was determined by Student's *t* test.

RESULTS

stn^ts and *stn^8P1* distinctly alter levels of stonedA and stonedB at larval motor terminals

Both stoned proteins are enriched in presynaptic terminals of the embryonic and larval NMJ (Stimson et al., 1998; Fergestad et al., 1999). We examined the effects of stn^{ts} and stn^{8P1} on stonedA and stonedB levels at the larval motor terminal. The stn^{ts} mutation is predicted to cause only a single amino acid change in stonedA (Phillips et al., 2000). This mutation does not alter presynaptic levels of stonedA consistently, although we frequently observe reduced levels (Fig. 1; Stimson et al., 1998). This variability is seen among synapses in a particular preparation, not only between individual larvae. Surprisingly, even when stonedA levels appear relatively normal, stn^{ts} causes a marked reduction in stonedB levels (Fig. 1). This observation suggests the intriguing possibility that an ORF1 mutation alters stonedB levels because stonedA has a function that affects the stability of stonedB at nerve terminals.

The stn^{8P1} mutation has striking effects on the levels of both stoned proteins. The stn^{8P1} allele has been described as semilethal (Miklos et al., 1987; Petrovich et al., 1993), and, in our hands, adult stn^{8P1} males survive at a frequency of ~1% relative to their control siblings. These survivors are extremely lethargic and can be immobilized for 1–2 min by mechanical disturbances (such as tapping or shaking the vial). Viability and behavior of stn^{8P1} males are not complemented by *stoned* lethal alleles (such as stn^{13-120}) but are restored to wild-type by $Dp(1,Y)y^{+}Ymal^{+}$ (*Dp*), a modified Y chromosome containing region 20 of the X chromosome, which includes *stoned*. Both stonedA and stonedB (Fig. 1) are reduced to undetectable levels in the stn^{8P1} mutant, an observation consistent with the severe effects of stn^{8P1} on viability and behavior. Because the stn^{8P1} mutation removes all detectable stonedA and stonedB immunoreactivity from the larval NMJ, we anticipated that analysis of stn^{8P1} mutants would allow us to assess the effects of nearly complete *stoned* loss-of-function in the third instar larval motor synapse. This prepara-

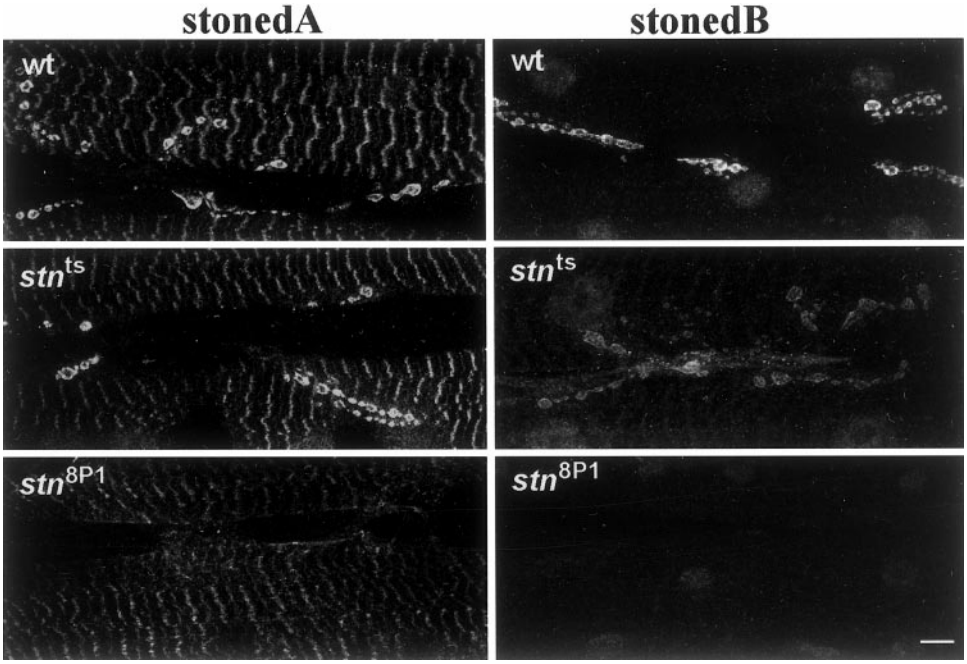

Figure 1. The levels of stonedA and stonedB at presynaptic terminals are altered distinctively in *stn* ts and *stn* 8P1 mutants. Shown are confocal micrographs of larval abdominal body wall muscles 6 and 7 stained with antibodies against stonedA and stonedB. StonedA and stonedB are enriched in presynaptic boutons of the wild-type larval NMJ. In *stn* ts boutons presynaptic levels of stonedA often appear similar to those in wild type, whereas levels of stonedB are reduced. In *stn* 8P1 boutons both stonedA and stonedB are not detectable above background staining. Scale bar, 10 μm.

tion has some advantages, as shown below, over the embryonic synapse in which the effects of other *stn* lethals have been analyzed previously (Fergestad et al., 1999).

stn 8P1 has distinct effects on larval synaptic physiology

To determine the effects of *stn* 8P1 on synaptic vesicle cycling, we first assessed the efficacy of synaptic transmission at the larval NMJ by performing intracellular recordings from postsynaptic muscle. We previously established that the *stn* ts mutant exhibits a threefold increase in the frequency of mejps, indicating an enhanced rate of spontaneous synaptic vesicle fusions (Stimson et al., 1998). However, mejp frequency in *stn* 8P1 is nearly identical to that of controls (3.6 ± 0.34 in *stn* 8P1, $n = 15$; 3.9 ± 0.42 in *stn* 8P1/*Dp*, $n = 13$). This observation probably is explained by reduced vesicle number and altered ultrastructure of mutant presynaptic terminals (documented later in this study).

EJPs evoked by stimulation of the motor nerve, normal in *stn* ts (Stimson et al., 1998), are reduced in *stn* 8P1 mutants to ~10% of wild-type and *stn* 8P1/*Dp* controls (Fig. 2). This decreased EJP amplitude derives from a severe reduction in quantal content, the number of synaptic vesicles fusing during a single evoked event. We calculated quantal content by dividing the EJP amplitude (corrected for nonlinear summation of individual quanta; Martin, 1955). Quantal content is only 4.7 ± 0.7 ($n = 14$) in *stn* 8P1 mutants as compared with 133.9 ± 16.1 ($n = 13$) in *stn* 8P1/*Dp* controls ($p = 4.3 \times 10^{-5}$). Thus, compared with other *stn* mutants that survive to the larval third instar (Stimson et al., 1998), stimulus-evoked synaptic vesicle fusion is limited severely at *stn* 8P1 neuromuscular synapses.

stn 8P1 alters the density and size of synaptic vesicles

Previous studies have indicated that altered neurotransmitter release in *stoned* mutants probably arises from a depletion of functional synaptic vesicles (Stimson et al., 1998; Fergestad et al., 1999). In *stoned* lethal mutants the boutons at the embryonic NMJ contain a relatively low density of synaptic vesicles, and many of these are morphologically abnormal (Fergestad et al., 1999). However, viable *stn* ts mutants with normal evoked release show no decrease in synaptic vesicle density and no change in synaptic vesicle size at the larval NMJ (Fig. 3; Stimson et al., 1998).

We found that in *stn* 8P1 mutants (Fig. 3) the boutons of the larval NMJ exhibit a 2.6-fold decrease in synaptic vesicle density as compared with controls ($p = 3 \times 10^{-4}$). Furthermore, we found that vesicles in *stn* 8P1 boutons are larger and more irregular in size than controls (Fig. 3). Vesicles in *stn* 8P1 average 44.8 ± 1.1 nm in diameter as compared with 34.4 ± 0.6 nm in *stn* 8P1/*Dp* controls, corresponding to approximately twofold increases in mean vesicle volume and in vesicle size variability ($p = 3.3 \times 10^{-16}$). Despite evidence from other studies that mejp amplitude often is correlated with vesicle size (Heuser, 1974; Fritz et al., 1980), we observed no increase in the average mejp amplitude or in the distribution of mejp amplitudes in *stn* 8P1 mutants (see Fig. 2*C–E*). This could indicate that the large vesicles of *stn* 8P1 are incompetent for fusion at the mature larval synapse. These morphological observations at larval motor terminals corroborate previous studies performed at the embryonic motor synapse. They are consistent with stoned proteins being essential for the formation of synaptic vesicles either during biogenesis or during recycling from the plasma membrane.

stn ts and *stn* 8P1 specifically alter the presynaptic localization of synaptic vesicle proteins

Light microscopic analysis of the distribution of synaptic vesicle proteins at embryonic motor terminals indicated that *stn* lethal mutations specifically alter the distribution of synaptotagmin (Syt). This suggested an intriguing hypothesis that stoned proteins act as specific adaptors for Syt (Fergestad et al., 1999). However, a preliminary examination of *stn* ts and *stn* c mutants reported that both Syt and Csp show altered distribution at the larval motor terminal (Stimson et al., 1998); a weakness of this study was that Syt and Csp distributions were not compared within the same terminal. Because a mechanistic hypothesis for how stoned proteins function depends significantly on establishing how *stn* mutations affect different vesicle proteins, we reexamined this issue in double-immunostained preparations. The large size of larval motor terminals permits substantial detail to

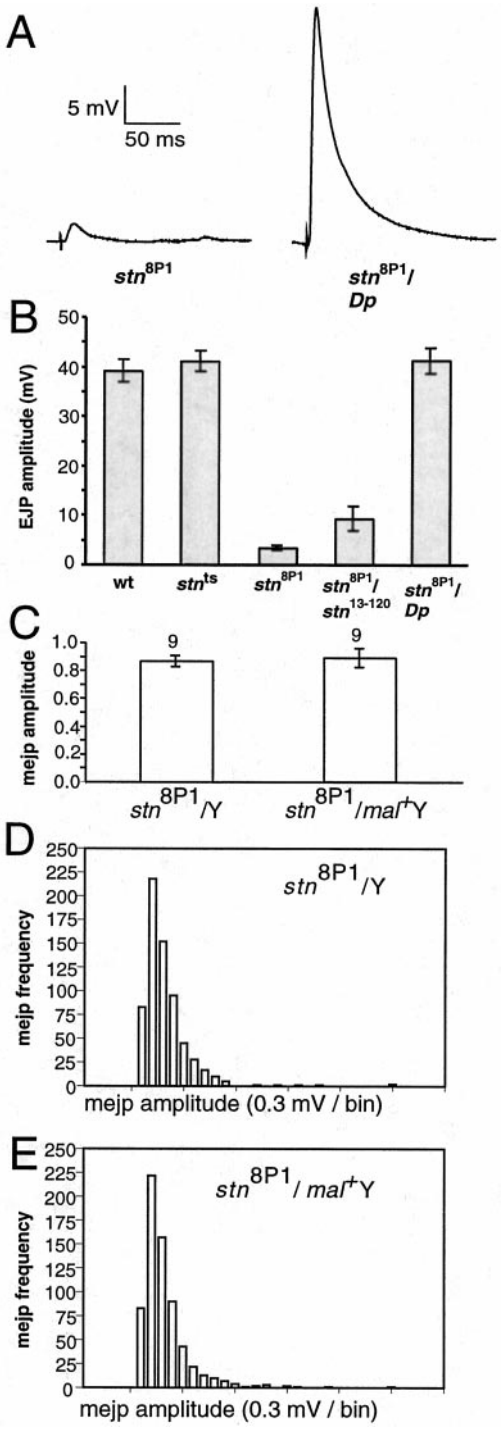

Figure 2. Evoked, but not spontaneous, neurotransmitter release is impaired severely in *stn* ^{8P1}. *A*, Measurements of postsynaptic responses evoked by nerve stimulation shown for *stn* ^{8P1} and *stn* ^{8P1}/*Dp*. *B*, EJP amplitudes are tabulated for other relevant genotypes. The reduced EJP phenotype of *stn* ^{8P1} is caused by a defect in *stoned* function because it is not complemented by the *stoned* lethal allele *stn* $^{13–120}$ and is complemented by a *stoned* duplication. EJP amplitude for *stn* ^{ts}, shown for comparison with the identical wild-type EJP amplitude, was reported previously in Stimson et al. (1998). In the graph, from *left* to *right*, the number of larvae examined was 22, 14, 14, 3, and 13 for the indicated genotype. *C*, MEJP sizes do not differ between *stn* ^{8P1} and *stn* ^{8P1}/*Dp*; thus, altered EJPs derive from reduced quantal content. *D, E*, Amplitude histograms for MEJP sizes in between *stn* ^{8P1} and *stn* ^{8P1}/*Dp* show essentially identical distributions. Significantly, there is no increase in the number of unusually large events in *stn* ^{8P1}.

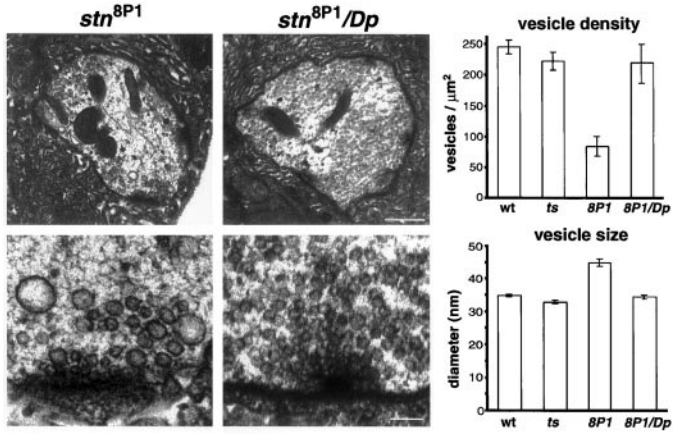

Figure 3. The *stn* ^{8P1} mutation alters synaptic vesicle number and size. Shown are electron micrographs (EMs) through motor terminals on larval body wall muscles 6 and 7. *Top panels*, *stn* ^{8P1} boutons have a lower density of synaptic vesicles than do controls. Scale bar, 500 nm. *Bottom panels*, High magnification views of active zones show that *stn* ^{8P1} boutons have abnormally large vesicles rarely observed in controls. Scale bar, 100 nm. Plots show that in *stn* ^{8P1} mutants the synaptic vesicle density is reduced significantly, whereas synaptic vesicle size is increased significantly. From *left* to *right*, the number of boutons examined was 46, 30, 19, and 17 for the indicated genotype.

be resolved by optical microscopy; specifically, plasma membrane and bouton interior may be discriminated clearly (Estes et al., 1996; Roos and Kelly, 1999).

In wild-type and control boutons, Syt and Csp are restricted to doughnut-shaped patterns surrounded by plasma membrane (Fig. 4*A,B*). However, in *stn* ^{8P1} mutants, Syt and Csp immunoreactivity is present diffusely over the boutons, colocalizes in the bouton periphery with plasma membrane staining, and invades interbouton regions of the motor terminal that usually are completely free of synaptic vesicle protein (Fig. 4*A,B*). Similar, although less pronounced, redistribution of Syt and Csp also is seen in double-stained *stn* ^{ts} boutons (data not shown). The observed distribution of these proteins in *stn* mutants is consistent with increased retention of Syt and Csp on presynaptic plasma membrane; the complex distribution pattern likely results from inefficient internalization and lateral movement of synaptic vesicle proteins along the axonal membrane (Jorgensen et al., 1995; Nonet et al., 1999). A particularly interesting observation is that, although both Csp and Syt are enriched on the plasma membrane of *stn* mutants, Syt shows much stronger immunoreactivity in the interbouton intervals than Csp (*arrowheads* in Fig. 4*A* show regions with relatively lower Csp staining). It is conceivable that the lateral movement of Csp away from boutons is restricted by physical interactions with presynaptic Ca^{2+} channels or other membrane proteins anchored within boutons (Mastrogiacomo et al., 1994). This observation offers an easy reconciliation of our findings with those of Fergestad et al. (1999), who described redistribution of Syt, but not Csp, to regions away from boutons but who did not comment on the distribution of these proteins *within* individual boutons. The significant redistribution of both Csp and Syt to the plasma membrane of larval motor terminals (Fig. 4) suggests that stoned proteins facilitate the sorting and assembly of at least two synaptic vesicle proteins into functionally mature synaptic vesicles. An immediate, rather than indirect, role for stoned proteins in these processes is argued by further immunolocalization studies shown in Figure 4*C*. Three known components of endocytosis,

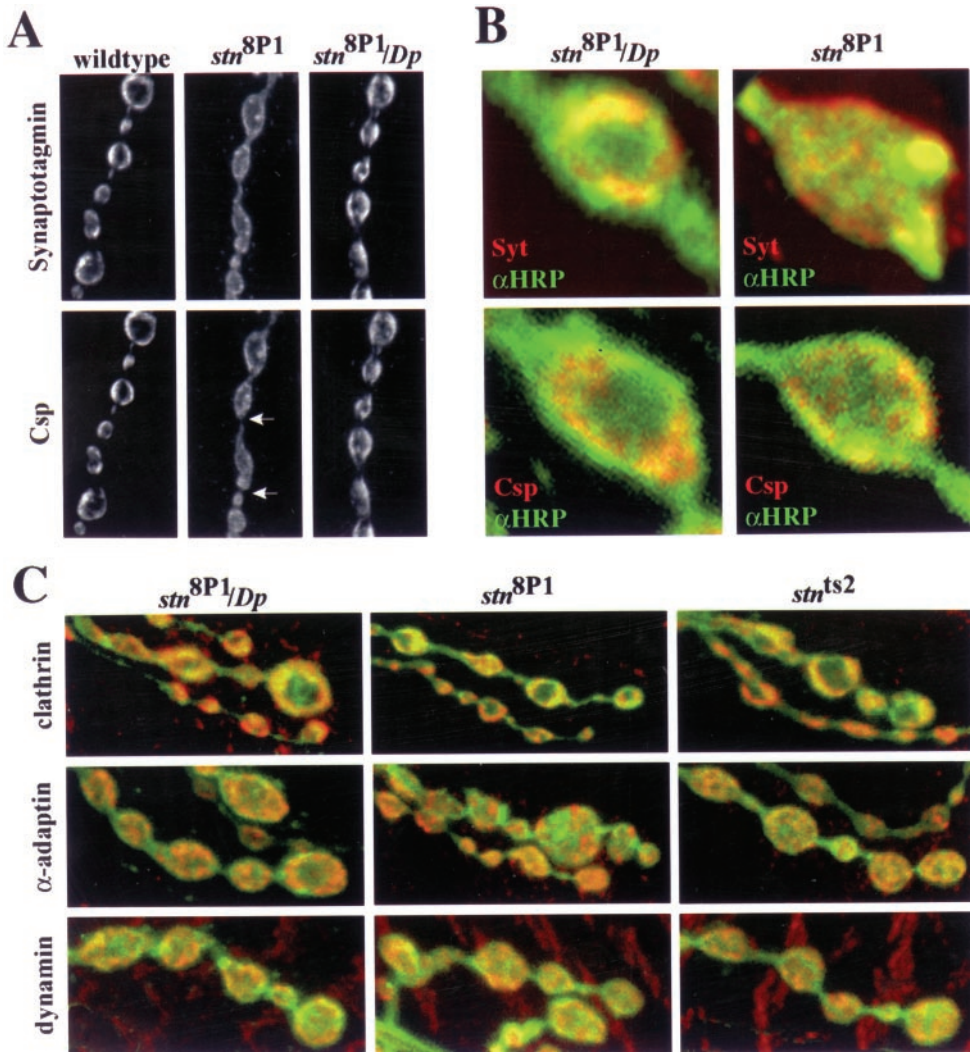

Figure 4. The *stn*^{8P1} mutation causes altered distribution of the synaptic vesicle proteins synaptotagmin (Syt) and cysteine string protein (Csp), but not of endocytosis proteins, clathrin heavy chain, α-adaptin, and dynamin within motor terminals. *A*, Lower magnification images of a string of boutons double-stained with antibodies against Syt (*top*) and Csp (*bottom*). *B*, High magnification images of single boutons double-stained with a plasma membrane label (anti-HRP, *green*) and anti-synaptotagmin (*red*; *top two panels*) or with anti-HRP (*green*) and Csp (*red*; *bottom two panels*). Syt and Csp, restricted to well defined subdomains within wild type, or control *stn*^{8P1}/*Dp* terminals, boutons, are distributed diffusely in *stn*^{8P1} mutant motor terminals (*A*). In wild-type and control terminals synaptic vesicle labeling is surrounded by plasma membrane that has been visualized by anti-HRP staining; however, in *stn*^{8P1} this labeling overlaps substantially in the bouton periphery with plasma membrane staining (*B*). The altered distribution patterns that are observed are consistent with the inefficient retrieval of Syt and Csp from the plasma membrane in *stn*^{8P1} mutants. *Arrows* indicate regions between boutons with low Csp immunoreactivity as compared with Syt (visible in the *paired image*). *C*, Images of larval motor terminals double-stained with anti-HRP (*green*) and each of three endocytosis proteins (*red*). The distribution of clathrin heavy chain (*top*), α-adaptin (*middle*), and dynamin (*bottom*) is not altered significantly in *stn*^{8P1} and *stn*^{ts} mutants. Thus, the altered localization of synaptic vesicle proteins reflects a function of *stoned* downstream of mechanisms that are involved in the expression and localization of endocytosis molecules. The boutons shown in *B* are ~4 μm in diameter.

α-adaptin, dynamin, and clathrin heavy chain, are not reduced significantly in levels or altered in distribution in *stn*^{ts} or *stn*^{8P1} mutant motor terminals. Thus, stoned proteins function downstream of the events required for expression and correct targeting of these endocytosis molecules, perhaps in the internalization process itself.

stn^{ts} enhances behavioral and physiological phenotypes of *shi*^{ts} mutants by slowing the rate of synaptic vesicle recycling

Phenotypes of *stoned* mutants described above could arise formally from defective synaptic vesicle biogenesis at the cell body. Abnormally sized vesicles might have arisen easily from the Golgi complex, and not from plasma membrane. Altered sorting, budding, and transport of synaptic vesicle components from the Golgi complex also could cause synaptic vesicle proteins to be targeted to the plasma membrane by a default sorting pathway. Abnormal fusion of presynaptic vesicles also might be a source for large presynaptic vesicles. To establish more firmly a role for stoned proteins in vesicle recycling from the plasma membrane, we performed a detailed analysis of phenotypes more directly associated with endocytosis at nerve terminals.

First, we further explored genetic interactions of *stn*^{ts} with *shi*^{ts} mutations that disrupt synaptic vesicle recycling. Specifically, we tested the effects of *stn*^{ts} on rapid temperature-sensitive paralysis of *shi*^{ts}, a phenotype believed to reflect synaptic failure directly.

Although *shi*^{ts1}–*stn*^{ts} double mutants are lethal, combining *stn*^{ts} with *shi* alleles weaker than *shi*^{ts1}, including *shi*^{ts2} and *shi*^{ts4}, produces viable *shi*^{ts}–*stn*^{ts} double mutants. Wild-type flies do not paralyze at sublethal temperatures (<42°C). Mutant *stn*^{ts} flies are sluggish but do *not* show temperature-sensitive paralytic behavior. In contrast, *shi*^{ts2} and *shi*^{ts4} flies show tight and complete paralysis in 2 min at 28 and 29°C, respectively (Fig. 5*A*). Double mutant *shi*^{ts2}–*stn*^{ts} and *shi*^{ts4}–*stn*^{ts} flies undergo paralysis at 26°C (Fig. 5*A*), a temperature 2–3°C below the restrictive temperature for *shi*^{ts} alone. Our observation that *stn*^{ts} lowers the temperature required to induce paralysis of *shi*^{ts} mutants adds to the previous discovery of synthetic lethality between *stn*^{ts} and *shi*^{ts1} (Petrovich et al., 1993). It suggests that *stn*^{ts} aggravates synaptic transmission defects in *shi*^{ts} mutants rather than defects in the various nonsynaptic functions of *shi*. The specificity of the *shi*^{ts}–*stn*^{ts} genetic interactions is emphasized by control double mutant studies that show the absence of any interaction of *stn*^{ts} with *para*^{ts1} and *comatose*^{tp7} (*comt*^{tp7}), temperature-sensitive paralytic mutants defective for action potential propagation (Loughney et al., 1989) and synaptic vesicle fusion (Pallanck et al., 1995), respectively (Fig. 5). In addition, *comt*^{ts} alleles have no effect on the temperature of paralysis of *shi*^{ts} (data not shown).

To confirm our cell biological interpretation of the behavioral interactions, we directly assessed the effects of *stn*^{ts} on synaptic vesicle recycling in *shi*^{ts} mutants. In *shi*^{ts} mutants the physiolog-

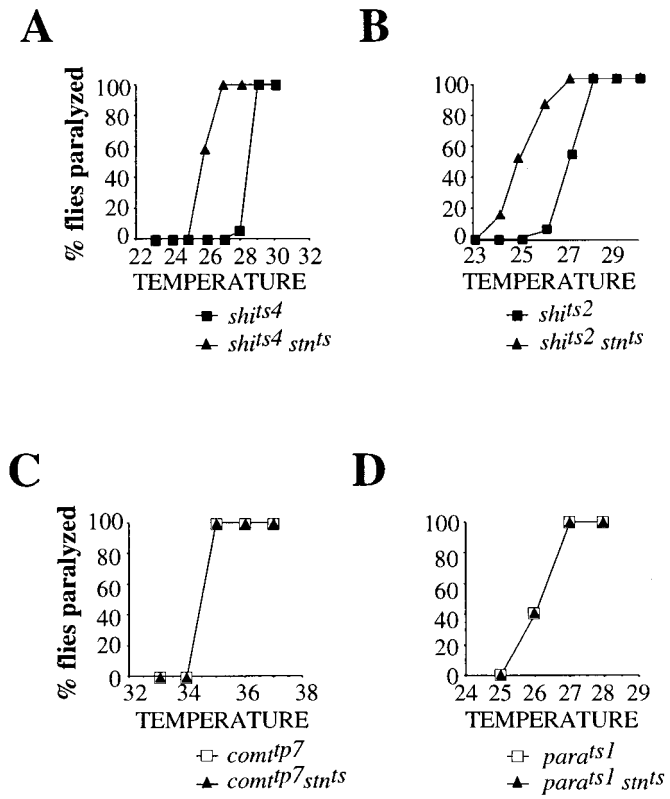

Figure 5. *Stn*^{ts} specifically enhances the temperature-sensitive paralysis of *shi*^{ts} mutants. The fraction of flies paralyzed in 2 min of exposure to specific temperatures is plotted as a function of temperature. *A, B*, *Stn*^{ts} lowers the temperature of paralysis of two *shi*^{ts} mutants, *shi*^{ts4} (*A*) and *shi*^{ts2} (*B*). This effect of *stn*^{ts} is specific to *shi*^{ts}; *stn*^{ts} has no effect on the behavior of two other paralytic mutants, *para*^{ts1} (*D*) and *comt*^{tp7} (*C*), which are defective in action potential propagation and synaptic vesicle fusion, respectively.

ical consequence of synaptic vesicle depletion is synaptic depression, an activity-dependent decline in quantal content over time (Koenig et al., 1989). We expected that, if *stn*^{ts} inhibits synaptic vesicle recycling, it should enhance synaptic depression caused by a partial inhibition of recycling in *shi*^{ts2} mutants. These depression experiments are uniquely possible in *shi*^{ts}–*stn*^{ts} double mutants because, unlike all other characterized *stoned* alleles, *stn*^{ts} does not alter EJP amplitude or vesicle number (Stimson et al., 1998; Fergestad et al., 1999). Thus, effects on vesicle recycling may be assayed without confounding effects from altered vesicle number or probability of release.

Because *shi*^{ts} mutations have obvious effects on the behavior of adult flies, the effects of *shi*^{ts} on synaptic physiology have been investigated most extensively at an adult fly NMJ on the dorsal longitudinal flight muscles (DLMs) (Salkoff and Kelly, 1978; Koenig and Ikeda, 1983; Koenig et al., 1989). To investigate the effects of *stn*^{ts} on *shi*^{ts2} depression, we optimized conditions for inducing depression at the larval NMJ of *shi*^{ts2} mutants (see Materials and Methods). With 10 Hz stimulation at 28°C the *shi*^{ts2} larval NMJ shows only a slight depression relative to the wild-type NMJ (Fig. 6*B*). Raising the temperature to 30°C causes a sharp distinction to emerge between *shi*^{ts2} and wild type. At 30°C, 10 Hz stimulation of the *shi*^{ts2} larval NMJ causes the EJP to decline from ~31 mV (~145 quanta) to ~9 mV (~30 quanta) after ~9 min (Fig. 6*A2,C*). In contrast, this 2° temperature change has no effect on the wild-type NMJ, which continues to show relatively robust synaptic transmission at 30°C (Fig. 6*A1,C*). Thus, these experiments establish that, at the larval NMJ, the *shi*^{ts2} mutation causes a weak inhibition of synaptic vesicle recycling at 28°C, but a strong inhibition at 30°C.

Identical experiments performed on *stn*^{ts} mutants provided only tentative support for the proposal that *stn*^{ts} affects synaptic vesicle recycling. Like *shi*^{ts2}, *stn*^{ts} alone at 28°C causes a marginal increase in the rate of synaptic depression as compared with wild type (Fig. 6*D*). However, unlike the case for *shi*^{ts2}, the effect of *stn*^{ts} on depression remains slight even at 30°C (Fig. 6*E*). Thus, in isolation, *stn*^{ts} shows only a marginal temperature-insensitive effect on synaptic depression; this observation is consistent with a model in which *stn*^{ts} causes a small reduction in the rate of synaptic vesicle recycling at larval NMJs.

We then examined whether this slight reduction in recycling rate would be made more obvious in a "sensitized" *shi*^{ts} background under conditions in which the vesicle recycling is slowed down already. Such analyses comparing *shi*^{ts2}–*stn*^{ts} double mutants with *shi*^{ts2} show that the *stn*^{ts} mutation has obvious effects on vesicle depletion in response to 10 Hz stimulation (Fig. 6). At 28°C, *stn*^{ts} causes a marked enhancement of the weak depression produced by *shi*^{ts2} alone (Fig. 6*F*), an effect that parallels the enhancement of *shi*^{ts2} paralysis by *stn*^{ts} (see Fig. 5*B*). Genetic control experiments show that both effects are caused specifically by *stn*^{ts}, and not by extragenic modifiers; thus, *shi*^{ts2} *stn*^{ts}; *shi*^{ts2} *stn*$^{13–120}$ mutants show depression and paralysis profiles identical to those of *shi*^{ts2}–*stn*^{ts} (Fig. 6*F*; data not shown). In principle, enhanced vesicle depletion may be caused by a smaller initial vesicle pool size (being depleted more quickly) or by slower vesicle recycling. Analyses performed at 30°C distinguish between these possibilities and show that *stn*^{ts} slows down vesicle recycling (Fig. 6*G*). If *stn*^{ts} accelerates synaptic vesicle depletion by limiting the initial pool of releasable synaptic vesicles, then even at 30°C, where *shi*^{ts2} strongly inhibits synaptic vesicle recycling, enhanced depression in *shi*^{ts2}–*stn*^{ts} would be expected. On the contrary, at 30°C, *stn*^{ts} has no detectable effect on the rate of *shi*^{ts2} depression (Fig. 6*G*), probably because the strong effects of *shi*^{ts2} on synaptic vesicle recycling mask more subtle effects of *stn*^{ts}. Because *stn*^{ts} alone shows marginal temperature-independent depression, the best explanation for enhanced temperature-dependent depression in *stn*^{ts}–*shi*^{ts2} double mutants is that stoned proteins facilitate synaptic vesicle recycling. This role is made visible by our analysis of *stn* function under sensitized conditions in which the recycling rate limits the efficiency of sustained transmitter release.

stn^{ts} slows synaptic vesicle recycling by slowing the rate of vesicle internalization from the plasma membrane

We next sought to determine the specific stage of synaptic vesicle recycling that is affected by stn^{ts}. Because sequence analysis and genetic interactions with *shi* suggest that stoned proteins act during membrane internalization, we implemented an assay that uses the fluorescent lipophilic dye FM1-43 to monitor the rate of synaptic vesicle internalization optically (Fig. 7*A*; Ryan et al., 1993). Because FM1-43 has a weak affinity for lipid membranes, bath-applied FM1-43 associates with the exposed lumenal surfaces of vesicles and becomes internalized into synaptic terminals during endocytosis (Betz et al., 1992). After washing away non-internalized plasma membrane-associated FM1-43, we can use the fluorescence intensity of internalized FM1-43 to quantify the amount of endocytosis.

To induce large-scale synaptic vesicle endocytosis, we sub-

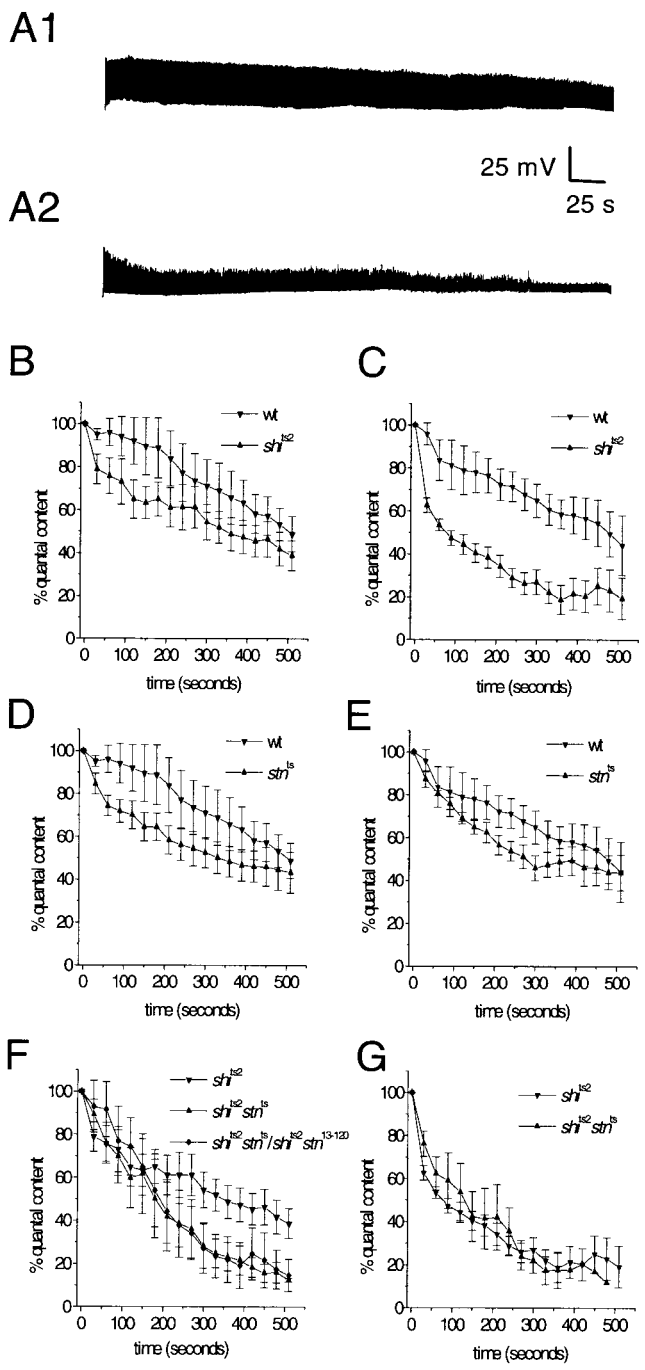

Figure 6. *Stn*^{ts} enhances the rate of synaptic vesicle depletion at *shi*^{ts2} synapses, indicating a specific effect on recycling. *A1, A2*, At a restrictive temperature for *shi*^{ts2} mutants, high frequency stimulation causes synaptic depression, a sign of synaptic vesicle depletion. *A1*, With 10 Hz stimulation at 30°C, wild-type NMJs can maintain synaptic transmission for several minutes but eventually will show some depression (see *B*). *A2*, In contrast, *shi*^{ts2} NMJs treated under the same conditions show a rapid decline in synaptic transmission. *B–G*, Synaptic depression profiles for wild-type, *shi*^{ts2}, and *shi*^{ts2}–*stn*^{ts} double mutants at 28°C (*left panels*) and 30°C (*right panels*). *B, C*, Synaptic depression in *shi*^{ts} mutants is temperature-dependent; at 28°C *shi*^{ts2} has only a marginal effect on the rate of depression, indicating weak inhibition of synaptic vesicle recycling. *D, E*, In a wild-type background *stn*^{ts} shows only a marginal effect on synaptic depression that is not affected by temperature. *F*, However, in a *shi*^{ts2} mutant background *stn*^{ts} causes a significant acceleration of synaptic depression at 28°C. Thus, *stn*^{ts} enhances the weak inhibition of synaptic vesicle recycling that is caused by *shi*^{ts2} at 28°C. This effect of *stn*^{ts} is not complemented by the lethal *stoned* allele *stn*$^{13–120}$ and, thus, is attributable specifically to loss of *stoned* function. *G*, At 30°C, where *shi*^{ts2} strongly inhibits synaptic vesicle recycling, there is no detectable effect of *stn*^{ts} on depression. This observation indicates that *stn*^{ts} affects the same synaptic function (vesicle recycling) as *shi*; thus, when recycling is blocked completely, no further effects of *stn*^{ts} are visible. Five to seven larvae were examined for each genotype, with the exception of *shi*^{ts2} *stn*^{ts}/*shi*^{ts2} *stn*$^{13–120}$, for which four larvae were examined.

jected the larval NMJ to a 30 sec, 30 Hz stimulation "buzz" (Fig. 7*A*). To measure endocytosis, we applied FM1-43 either just before the buzz or at incremental time points after the buzz (t = 0 and t = 1 min) and then allowed at least 5 min for endocytosis to run to completion before washing away noninternalized FM1-43 (Fig. 7*A*). Adding FM1-43 just before the stimulation labels those synaptic vesicles that have been released and recycled consequent to the stimulation ("max" staining). FM1-43 added after the stimulation (at t = 0 and t = 1 min) labels only those synaptic vesicles that recycle relatively slowly from the plasma membrane, whereas vesicles that have internalized before the dye application escape labeling. By making quantitative fluorescence measurements at each time point, we can use this assay to determine the rate of synaptic vesicle endocytosis. Furthermore, by normalizing the t = 0 and t = 1 min measurements to max dye uptake for each respective genotype, we can eliminate variability in the amount of evoked and spontaneous exocytosis (a potential concern in *stn*^{ts} mutants) from the analysis.

The assay shows that synaptic vesicle internalization in *stn*^{ts} mutants is delayed relative to wild type. In *stn*^{ts} boutons intense FM1-43 uptake persists after the 30 Hz stimulation has ended, whereas in wild-type boutons FM1-43 uptake rapidly wanes after stimulation (Fig. 7*B*). Normalized fluorescence intensities show that, whereas only ~40% of vesicle membrane in wild-type boutons remains to be internalized after stimulation, >60% of vesicle membrane in *stn*^{ts} boutons is internalized after stimulation (Fig. 7*C*). At 1 min after stimulation, in which the FM1-43 uptake is barely detected in wild-type boutons (Fig. 7*B,C*), the difference between wild type and *stn*^{ts} is especially pronounced. This phenomenon, obvious in *stn*^{ts}, is even stronger in *stn*^{ts}/*stn*$^{13–120}$ heterozygotes, indicating that delayed vesicle internalization is caused by a mutation in *stoned* (Fig. 7*C*). Delayed vesicle internalization in the *stn*^{ts} mutant indicates that stoned proteins facilitate synaptic vesicle recycling by promoting endocytosis from the presynaptic plasma membrane.

DISCUSSION

Phenotypes of *stn*^{ts} and *stn*^{8P1} provide new insights into *stoned* function

The *stn*^{ts} mutation has no effect on evoked neurotransmitter release or ultrastructure at the larval NMJ (Stimson et al., 1998). The consequently normal level of evoked synaptic transmission in *stn*^{ts} thus allowed us to examine subtle alterations in synaptic vesicle recycling that would have been difficult to assess in mutants with severe transmission defects. In contrast, *stn*^{8P1} is a strong loss-of-function mutation that severely decreases evoked neurotransmitter release (see Fig. 2), decreases synaptic vesicle density, and increases synaptic vesicle size (see Fig. 3). Thus, our analysis of *stn*^{8P1} demonstrates that loss of *stoned* function has qualitatively similar effects on the embryonic (Fergestad et al., 1999) and the larval NMJs. However, the larger size of larval terminals allowed us to examine the redistribution of two different *Drosophila* synaptic vesicle membrane proteins within indi-

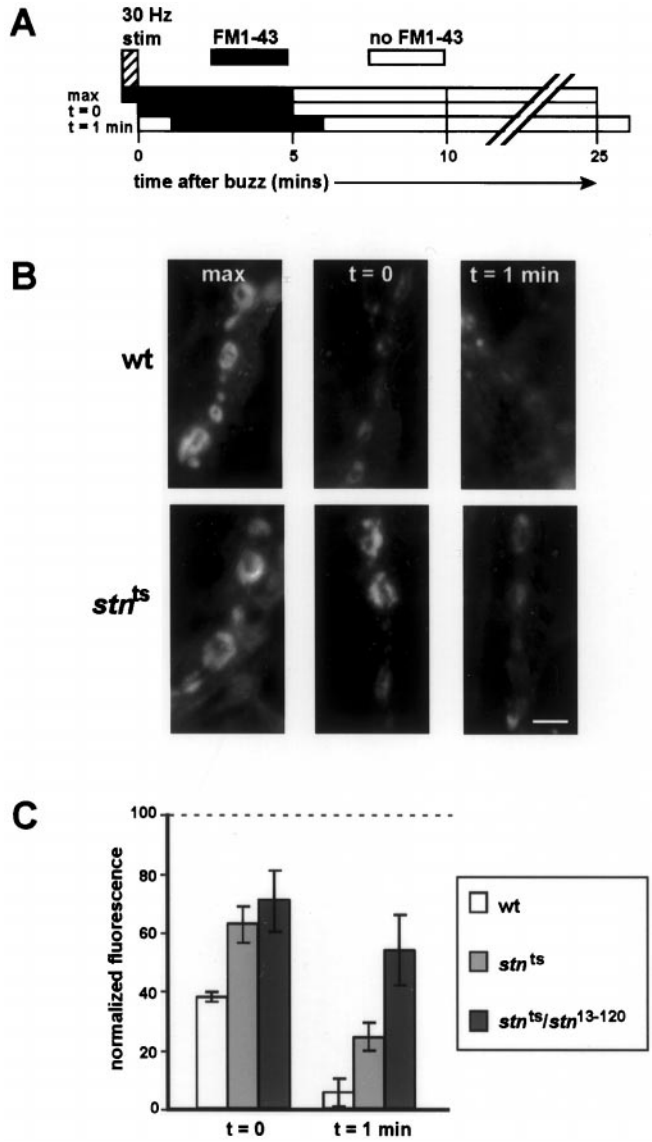

Figure 7. *Stn*^{ts} slows the rate of synaptic vesicle internalization. *A*, Our protocol for measuring the rate of synaptic vesicle endocytosis. The NMJ is subjected to 30 Hz stimulation for 30 sec to induce a burst of exocytosis. FM1-43 applied just before stimulation labels the complete exo–endo cycling pool of synaptic vesicles. FM1-43 applied at $t = 0$ and $t = 1$ min after stimulation labels only those vesicles that have been internalized after these time points. *B*, A time course of FM1-43 labeling at wild-type and *stn*^{ts} boutons. After stimulation the *stn*^{ts} boutons appear to take up more dye than wild-type boutons, indicating significantly delayed vesicle internalization. Scale bar, 5 μm. *C*, Quantitative fluorescence measurements of FM1-43 labeling (normalized to maximal uptake for each genotype, as described in Materials and Methods) show that FM1-43 uptake is prolonged at *stn*^{ts} boutons, indicating that synaptic vesicle endocytosis is delayed. This delay is specifically attributable to loss of *stoned* function, because it is even more pronounced in *stn*^{ts}/*stn*$^{13-120}$ mutants. For each genotype three to seven larvae were examined under each condition. A fresh larva was used for each experiment; thus, one bouton provides a single data point (see Materials and Methods).

vidual boutons of this severe *stn* mutant. Our combined analysis of *stn*^{ts} and *stn*^{8P1} mutants provides several new insights into *stoned* function, including possible interaction between the stoned proteins, their role in synaptic vesicle recycling, and their functional similarity to adaptor proteins.

Coordinate expression and function of the stoned proteins

Although unrelated by sequence, the *Drosophila* stoned proteins are translated from a single dicistronic mRNA, transcribed under the control of a single genetic promoter (Andrews et al., 1996). This arrangement resembles the polycistronic RNAs commonly found in prokaryotes, which are known to facilitate the coexpression of gene products that act in a common pathway (Blumenthal, 1998). Simply based on the molecular organization of *stoned*, it is a logical extension that stonedA and stonedB proteins are expressed coordinately because they share some overall function (Andrews et al., 1996). A more speculative idea is that coordinate expression of stonedA and stonedB promotes physical interaction between them by increasing their local concentrations (Blumenthal, 1998).

Our analysis of stonedA and stonedB immunoreactivity in *stn* mutants provides some supportive evidence for both of these possibilities. Previously analyzed *stn* alleles either reduce levels of presynaptic stonedA and stonedB or else carry specific lesions in ORF2 (Stimson et al., 1998; Fergestad et al., 1999). These studies suggested that mutations in ORF1 interfere with the translation of stonedA and stonedB (Fergestad et al., 1999). Contrary to this suggestion, we have found that *stn*^{ts}, a missense mutation in ORF1, severely reduces stonedB levels even when stonedA levels are only marginally affected, as judged by immunofluorescence analysis (see Fig. 1). Thus, *stn*^{ts} appears to have a primary effect on stonedA function, not expression, and a secondary effect on the presence of stonedB in presynaptic boutons. This suggests that mutations of stonedA alter the abundance of stonedB because stonedA protein regulates the transport and/or stability of stonedB within presynaptic terminals. The interdependence of stonedA and stonedB observed *in vivo* reinforces the notion that stonedA and stonedB share common functions. Such a model is supported by sequence analysis, indicating the presence in stonedA of μ-adaptin binding sequences and in stonedB of a μ-adaptin homology domain as well as PEST sequences that target proteins for turnover in the absence of protective interactions. Recent biochemical studies also provide some support for a model in which stonedA and stonedB associate in a single macromolecular complex at some stage of synaptic vesicle traffic (Phillips et al., 2000).

The stoned proteins regulate synaptic vesicle recycling

In the context of sequence motifs present in stoned proteins, phenotypes of *stoned* mutants, combined with the enrichment of stonedA and stonedB in presynaptic boutons, specifically suggest that the stoned proteins regulate the recycling of synaptic vesicles. Previously described *stoned* phenotypes, namely the mislocalization of synaptic vesicle proteins as well as the enlargement and depletion of synaptic vesicles, provide strong support for the proposal that stonedA and stonedB promote synaptic vesicle recycling. Similar phenotypes have been observed in the *Drosophila* and *Caenorhabditis elegans* mutant for AP180 (Zhang et al., 1998; Nonet et al., 1999), an adaptor protein that regulates the assembly of clathrin cages (Ye and Lafer, 1995) and colocalizes with clathrin on budding vesicles (Takei et al., 1996). Although these data are consistent with a role for stoned in regulating recycling, the data fall short of demonstrating such a function. Given the relative paucity of information on the biochemical activities of stoned proteins, direct data are especially important to support the hypothesis that the proteins regulate vesicle formation. For this reason, we developed new methods to assess

directly the rates of synaptic vesicle recycling and synaptic vesicle internalization in *Drosophila*.

We used *shi*^{ts} mutations as tools to probe the specific effects of the *stn*^{ts} mutation on synaptic vesicle recycling. Our analysis shows that *stn*^{ts} can enhance paralysis (and the underlying synaptic depression) caused by *shi*^{ts} inhibition of synaptic vesicle recycling (see Figs. 5, 6). Further studies under conditions in which the recycling is blocked almost completely exclude the formal possibility that *stn*^{ts} accelerates synaptic vesicle depletion by reducing the size of the initial vesicle pool. Thus, *stn*^{ts} enhancement of *shi*^{ts} depression, detectable when the inhibitory effects of *shi*^{ts} are weak (see Fig. 6*F*), is not apparent when the effects are strong (see Fig. 6*G*). This constitutes the first direct evidence that stoned proteins modulate synaptic vesicle recycling.

Interpreted from a genetic standpoint, the finding that *shi*^{ts} can mask the effect of *stn*^{ts} (i.e., *shi*^{ts} is epistatic to *stn*^{ts}) suggests that the stoned proteins function in the same cellular pathway as dynamin, probably as novel components of endocytic vesicle formation.

The stoned proteins promote internalization of synaptic vesicle components from the plasma membrane

Although recent evidence suggests that mature synaptic vesicles are reassembled entirely during internalization from plasma membrane (Murthy and Stevens, 1998), it is possible that *stoned* modulation of vesicle recycling occurs during unidentified membrane traffic events subsequent to membrane internalization. For instance, stoned proteins might participate in an alternate recycling pathway, wherein synaptic vesicle components are sorted at internal membrane compartments called endosomes (Heuser and Reese, 1973; Koenig and Ikeda, 1989), or stoned proteins could be part of an unidentified mechanism to prevent homotypic fusion of endocytic vesicles after internalization.

To assess directly the efficiency of membrane internalization in *stn*^{ts} mutants, we measured the rate of synaptic vesicle internalization by monitoring the presynaptic uptake of the lipophilic dye FM1-43 (Betz and Bewick, 1992; Ryan et al., 1993; Wu and Betz, 1998). Our finding that the bulk of FM1-43 uptake is delayed in *stn*^{ts} boutons (see Fig. 7) shows that *stn*^{ts} slows the rate of synaptic vesicle endocytosis from the plasma membrane. These data do not exclude the possibility that altered synaptic vesicle internalization is a secondary consequence of a defect in vesicle biogenesis, but they significantly strengthen a model in which the stoned proteins, like other adaptor proteins AP-2 and AP180, directly participate in synaptic vesicle internalization from plasma membrane.

Consistent with defects in synaptic vesicle internalization, all *stoned* mutants we have examined exhibit an accumulation of two synaptic vesicle proteins, Syt and Csp, on the presynaptic plasma membrane at the larval NMJ (see Fig. 4; data not shown). From their examination of embryonic boutons in several *stoned* mutants, Fergestad et al. (1999) reported altered presynaptic distribution of Syt, but not Csp. It is likely that immunovisualization of embryonic boutons, which have a maximum diameter of 1 μm (Prokop, 1999), does not allow for the optical resolution required to distinguish bouton plasma membrane from intrabouton clusters of synaptic vesicles. This is feasible at large (3–5 μm) third instar larval boutons (Atwood et al., 1993; Estes et al., 1996; Johansen et al., 1989; Roos and Kelly, 1999; Wan et al., 2000). This increased resolution may be required for observing altered distribution of Csp that, when on plasma membrane, does not diffuse laterally into the interbouton region as efficiently as Syt. Regardless, of the mechanisms that underlie the restricted lateral diffusion of Csp, our observations show that Syt and Csp are both mislocalized to the presynaptic plasma membrane in *stn* mutant larvae, most likely because they are not internalized efficiently into nascent synaptic vesicles.

Previous studies suggested a model in which stoned proteins selectively recruit Syt into synaptic vesicles either during endocytosis or during subsequent unidentified trafficking events in synaptic vesicle recycling (Fergestad et al., 1999). Our findings that *stn* mutations slow the internalization of synaptic vesicle membrane and disrupt the retrieval of at least two synaptic vesicle proteins allow us to refine this model of stoned function. In this revised model we suggest that stoned proteins are novel components of endocytosis that promote the recovery of synaptic vesicle membrane and proteins from the presynaptic plasma membrane. In support of this, both stonedA and stonedB bind Syt *in vitro* (Phillips et al., 2000), stonedA contains consensus binding sites for α-adaptin (Stimson et al., 1998; Owen et al., 1999), and stonedB contains consensus binding sites for Eps15 (Salcini et al., 1997). Although biochemical properties of stonedA and stonedB are not firmly established, new analyses presented here show that stoned proteins have the functional characteristics expected of molecules involved in synaptic vesicle internalization. Together, the available data suggest a model in which stoned proteins physically link synaptic vesicle proteins with components of the clathrin-associated endocytosis machinery during synaptic vesicle reformation.

REFERENCES

Andrews J, Smith M, Merakovsky J, Coulson M, Hannan F, Kelly LE (1996) The *stoned* locus of *Drosophila melanogaster* produces a dicistronic transcript and encodes two distinct polypeptides. Genetics 143:1699–1711.

Atwood HL, Govind CK, Wu C-F (1993) Differential ultrastructure of synaptic terminals on ventral longitudinal abdominal muscles in *Drosophila* larvae. J Neurobiol 24:1008–1024.

Betz WJ, Bewick GS (1992) Optical analysis of synaptic vesicle recycling at the frog neuromuscular junction. Science 255:200–203.

Betz WJ, Mao FM, Bewick GS (1992) Activity-dependent fluorescent staining and destaining of living vertebrate motor nerve terminals. J Neurosci 12:363–375.

Blumenthal T (1998) Gene clusters and polycistronic transcription in eukaryotes. BioEssays 20:480–487.

Chen YS, Obar RA, Schroeder CC, Austin TW, Poodry CA, Wadsworth SC, Vallee RB (1991) Multiple forms of dynamin are encoded by the *shibire*, a *Drosophila* gene involved in endocytosis. Nature 351:583–586.

De Camilli P, Takei K (1996) Molecular mechanisms in synaptic vesicle endocytosis and recycling. Neuron 16:481–486.

Estes P, Roos J, van der Bliek A, Kelly R, Krishnan K, Ramaswami M (1996) Traffic of dynamin within individual *Drosophila* synaptic boutons relative to compartment-specific markers. J Neurosci 16:5443–5456.

Fergestad T, Davis WS, Broadie K (1999) The stoned proteins regulate synaptic vesicle recycling in the presynaptic terminal. J Neurosci 19:5847–5860.

Fritz LC, Atwood HL, Jahromi SS (1980) Lobster neuromuscular junctions treated with black widow spider venom: correlation between ultrastructure and physiology. J Physiol (Lond) 9:699–721.

Gonzalez-Gaitan M, Jackle H (1997) Role of *Drosophila* α-adaptin in presynaptic vesicle recycling. Cell 88:767–776.

Grant D, Unadkat S, Katzen A, Krishnan KS, Ramaswami M (1998) Probable mechanisms underlying interallelic complementation and temperature sensitivity of mutations at the *shibire* locus of *Drosophila melanogaster*. Genetics 149:1019–1030.

Grigliatti T, Hall L, Rosenbluth R, Suzuki DT (1973) Temperature-sensitive mutations in *Drosophila melanogaster*. XIV. A selection of immobile adults. Mol Gen Genet 120:107–114.

Heuser J (1974) Proceedings: a possible origin of the "giant" spontaneous potentials that occur after prolonged transmitter release at frog neuromuscular junctions. J Physiol (Lond) 239:106P–108P.

Heuser J, Reese T (1973) Evidence for recycling of synaptic vesicle membrane during transmitter release at the frog neuromuscular junction. J Cell Biol 57:315–344.

Johansen J, Halpern ME, Johansen KM, Keshishian H (1989) Stereo-

typic morphology of glutamatergic synapses on identified muscle cells of *Drosophila* larvae. J Neurosci 9:710–725.
Jorgensen E, Hartwieg E, Schuske K, Nonet M, Jin Y, Horvitz H (1995) Defective recycling of synaptic vesicles in synaptotagmin mutants of *Caenorhabditis elegans*. Nature 378:196–199.
Keshishian H, Broadie K, Chiba A, Bate M (1996) The *Drosophila* neuromuscular junction: a model system for studying synaptic development and function. Annu Rev Neurosci 19:545–575.
Koenig JH, Ikeda K (1983) Evidence for a presynaptic blockage of transmission in a temperature-sensitive mutant of *Drosophila*. J Neurobiol 14:411–419.
Koenig JH, Ikeda K (1989) Disappearance and reformation of synaptic vesicle membrane upon transmitter release observed under reversible blockage of membrane retrieval. J Neurosci 9:3844–3860.
Koenig J, Kosaka T, Ikeda K (1989) The relationship between the number of synaptic vesicles and the amount of neurotransmitter released. J Neurosci 9:1937–1942.
Littleton TJ, Pallanck L, Ganetzky B (1999) Mechanisms of neurotransmitter release. In: Neuromuscular junctions in *Drosophila* (Budnik V, Gramates LS, eds), pp 139–161. San Diego: Academic.
Loughney K, Kreber R, Ganetzky B (1989) Molecular analysis of the *para* locus, a sodium channel gene in *Drosophila*. Cell 58:1143–1154.
Martin A (1955) A further study of the statistical composition of the end plate potential. J Physiol (Lond) 130:114–122.
Mastrogiacomo A, Parsons SM, Zampighi GA, Jenden DJ, Umbach JA, Gundersen CB (1994) Cysteine string proteins: a potential link between synaptic vesicles and presynaptic Ca^{2+} channels [see comments]. Science 263:981–982.
Miklos GLG, Kelly LE, Coombe PE, Leeds C, Lefevre G (1987) Localization of the genes *shaking-B*, *small optic lobes*, *sluggish-A*, *stoned*, and *stress-sensitive-C* to a well defined region of the X-chromosome of *Drosophila melanogaster*. J Neurogenet 4:1–19.
Murthy VN, Stevens CF (1998) Synaptic vesicles retain their identity through the endocytic cycle. Nature 392:497–501.
Nonet ML, Holgado AM, Brewer F, Serpe CJ, Norbeck BA, Holleran J, Wei L, Hartwieg E, Jorgensen EM, Alfonso A (1999) UNC-11, a *Caenorhabditis elegans* AP180 homologue, regulates the size and protein composition of synaptic vesicles. Mol Biol Cell 10:2343–2360.
Owen D, Vallis Y, Noble M, Hunter J, Daffron T, Evans P, McMahon H (1999) A structural explanation for the binding of multiple ligands by the α-adaptin appendage domain. Cell 97:805–815.
Pallanck L, Ordway RW, Ganetzky B (1995) A *Drosophila* NSF mutant [letter]. Nature 376:25.
Petrovich TZ, Merakovsky J, Kelly LE (1993) A genetic analysis of the *stoned* locus and its interaction with *dunce*, *shibire*, and *suppressor* of *stoned* variants of *Drosophila melanogaster*. Genetics 133:955–965.
Phillips AM, Smith M, Ramaswami M, Kelly LE (2000) Interactions between the products of the *Drosophila stoned* locus and the vesicle membrane protein, synaptotagmin. J Neurosci 20:8254–8261.
Prokop A (1999) Integrating bits and pieces: synapse structure and formation in *Drosophila* embryos. Cell Tissue Res 297:169–186.
Ramaswami M, Rao S, van der Bliek A, Kelly R, Krishnan K (1993) Genetic studies on dynamin function in *Drosophila*. J Neurogenet 9:73–87.
Robinson MS (1992) Adaptins. Trends Cell Biol 2:293–297.
Robinson MS (1994) The role of clathrin, adaptors, and dynamin in endocytosis. Curr Opin Cell Biol 6:538–544.
Roos J, Kelly RB (1999) The endocytic machinery in nerve terminals surrounds sites of exocytosis. Curr Biol 9:1411–1414.
Ryan T, Reuter H, Wendland B, Schweizer F, Tsien R, Smith S (1993) The kinetics of synaptic vesicle recycling measured at single presynaptic boutons. Neuron 11:713–724.
Salcini AE, Confalonieri S, Doria M, Santolini E, Tassi E, Minenkova O, Cesareni G, Pelicci PG, Di Fiore PP (1997) Binding specificity and *in vivo* targets of the EH domain, a novel protein–protein interaction module. Genes Dev 11:2239–2249.
Salkoff L, Kelly L (1978) Temperature-induced seizure and frequency-dependent neuromuscular block in a *ts* mutant of *Drosophila*. Nature 273:156–158.
Schmid SL, McNiven MA, De Camilli P (1998) Dynamin and its partners: a progress report. Curr Opin Cell Biol 10:504–512.
Shih W, Gallusser A, Kirchhausen T (1995) A clathrin-binding site in the hinge of the β2 chain of mammalian AP-2 complexes. J Biol Chem 270:31083–31090.
Stewart BA, Atwood HL, Renger JJ, Wang J, Wu C-F (1994) Improved stability of *Drosophila* larval neuromuscular preparations in haemolymph-like physiological solutions. J Comp Physiol [A] 175:179–191.
Stimson DT, Estes PS, Smith M, Kelly LE, Ramaswami M (1998) A product of the *Drosophila stoned* locus regulates neurotransmitter release. J Neurosci 18:9638–9649.
Takei K, McPherson PS, Schmid S, De Camilli P (1995) Tubular membrane invaginations coated by dynamin rings are induced by GTPγS in nerve terminals. Nature 374:186–190.
Takei K, Mundgihl O, Daniell L, De Camilli P (1996) The synaptic vesicle cycle: a single vesicle budding step involving clathrin and dynamin. J Cell Biol 133:1237–1250.
van der Bliek AM, Meyerowtiz EM (1991) Dynamin-like protein encoded by the *Drosophila shibire* gene associated with vesicular traffic. Nature 351:411–414.
Wan HI, DiAntonio A, Fetter RD, Bergstrom K, Strauss R, Goodman CS (2000) Highwire regulates synaptic growth in *Drosophila*. Neuron 26:313–329.
Warnock DE, Schmid SL (1996) Dynamin GTPase, a force-generating molecular switch. BioEssays 18:885–893.
Wu LG, Betz WJ (1998) Kinetics of synaptic depression and vesicle recycling after tetanic stimulation of frog motor nerve terminals. Biophys J 74:3003–3009.
Ye W, Lafer EM (1995) Clathrin binding and assembly activities of expressed domains of the synapse-specific clathrin assembly protein AP-3. J Biol Chem 270:10933–10939.
Zhang B, Koh YH, Beckstead RB, Budnik V, Ganetzky B, Bellen HJ (1998) Synaptic vesicle size and number are regulated by a clathrin adaptor protein required for endocytosis. Neuron 21:1465–1475.
Zhang JZ, Davletov BA, Sudhof TC, Anderson RGW (1994) Synaptotagmin I is a high affinity receptor for clathrin AP-2: implications for membrane recycling. Cell 78:751–760.